Acoustic source localisation using vibroacoustic beamforming

Mahmoud Karimi, Laurent Maxit

Acoustic Source Localisation using Vibroacoustic Beamforming

Mahmoud Karimi[1*], Laurent Maxit[2]

[1] *Centre for Audio, Acoustics and Vibration, University of Technology Sydney, Sydney, Australia*

[2] *Univ Lyon, INSA Lyon, LVA, 25 bis, av. Jean Capelle, 69621, Villeurbanne Cedex, France*

Abstract

For acoustic source localisation in a fluid, sound pressure is traditionally measured using a microphone array, and acoustic beamforming is then applied to the pressure signals to localise the source. However, in some engineering applications, it is not feasible to place the microphone/hydrophone array in the fluid to localise an acoustic source. Hence, this work proposes a vibroacoustic beamforming for sound source localisation which applies the beamforming procedure to the measured vibration signals at the surface of a structure in contact with the fluid in which the acoustic source is located. To evaluate the localisation performance of the proposed method, a numerical study is conducted to localise a monopole source in a room using vibration data obtained from an elastic panel on the room wall. To simulate more realistic situation, different levels of signal to noise ratio are considered by moving the source away from the wall-mounted sensors and consequently altering the direct acoustic field (signal). Moreover, commonly used frequency domain beamforming techniques namely conventional beamforming, functional beamforming, minimum variance distortionless response and minimum power distortionless response are applied to the measured signals to localise the source. The performance of each technique is then evaluated by comparing the beamforming output obtained from vibroacoustic beamforming with that of acoustic beamforming and by quantifying the dynamic range and spatial resolution for each method. It can be concluded that vibroacoustic beamforming can be used for acoustic localisation as an alternative to the acoustic beamforming.

Keywords: Sound source localisation, Vibroacoustic, Conventional beamforming, Functional beamforming, MVDR, MPDR

*Corresponding author

Email address: Mahmoud.karimi@uts.edu.au

1. INTRODUCTION

The advent of "acoustic telescopes" to identify ships in foggy weather was the first application of acoustic source localisation more than a century ago. The concept was that if the device was pointed in the direction of a sound source, sounds collected at receivers would arrive at the same time and so reinforce each other when the total sound was heard. In addition to ship and vehicle detection, acoustic source localisation has been used to provide guidelines on product noise control, target selection and interference rejection for communication devices or speech recognition processing, and noise source identification for mechanical systems. In general, sources are detected in beamforming by scanning all possible source locations and calculating the likelihood of an actual source at each probable spot based on the strength of the combined microphones' output signals. Chiariotti et al. [1] reviewed different acoustic beamforming (ABF) methods for source localisation in different applications. The main concepts of beamforming, starting from the very basics and progressing onto more advanced concepts and techniques along with application were presented. They briefly reviewed the most common beamforming methods. The so-called conventional beamforming (CBF), also known as delay-and-sum beamforming, is the most straightforward and reliable beamforming algorithm. As a result, it is most commonly employed in practice. The phase delays between the emission of the sound signal at the source and the received signals at each microphone are used in this technique. This approach can be used in the time domain or the frequency domain by applying a discrete Fourier transform to the data. Because of the reduced computing time and the ability to perform a frequency analysis, the latter is extensively employed. Deconvolution algorithms [2, 3], especially the DAMAS algorithm [4], are the main methods used in recent years to reconstruct a clean map of source distributions from a dirty map via iterative deconvolution, and thus can significantly improve the spatial resolution that cannot be achieved by traditional beamforming algorithms. However, their inevitable iteration nature results in much more computational complexity than traditional beamforming. Hence, some scholars abandoned the deconvolution algorithm, returned to the traditional beamforming algorithm and proposed some new beamforming algorithms, for example, adaptive beamforming [5] and functional beamforming [6].

Two most common adaptive beamforming techniques widely used in the literature are the MVDR (Minimum Variance Distortionless Response) and MPDR (Minimum power Distortionless Response). They both minimize output power under the constraint that the assumed steering vector goes non-distorted. The power minimization in MVDR only includes the effect of noise while both noise and desired signal are taken into account in MPDR [5]. Ehrenberg et al. [7] conducted a sensitivity

analysis of these two distortionless beamformers. The MVDR beamformer, which employs the noise correlation matrix as its minimisation criterion, was found to be more resilient to steering errors than the MPDR beamformer, which uses the received signal correlation matrix. Furthermore, even if the noise correlation matrix is computed incorrectly due to steering errors in the interference direction, the MVDR advantage is maintained for a fairly good range of steering errors. The performance of the adaptive beamforming technique degrades considerably as the steering vector and covariance matrix become inaccurate [8]. Carlson introduced a diagonal loading approach that pulsates a constant diagonal loading compensation value to the diagonal components of the covariance matrix to lower the dispersive degree of the eigenvalues of the covariance matrix [9].

Dougherty [10] recently proposed the functional beamforming (FBF). Despite its simplicity, it has been found to improve array spatial resolution and dynamic range. The computing time for functional beamforming is comparable to that of a typical frequency domain beamformer and far less than that of deconvolution methods. The name "functional beamforming" comes from the algorithm's use of functions of matrices. An exponent parameter is used in the algorithm. In a functional sense, the cross spectral matrix (CSM) is raised to the power of the reciprocal of this exponent. The adjusted CSM is then used in the CBF method, and the values of the resulting beamforming map are elevated to the non-reciprocal exponent's power. Array sidelobes are essentially avoided for big values of the exponent. This boosts array design flexibility and greatly increases the system's dynamic range, allowing new sources to be uncovered. FBF was successfully employed to landing aircraft fly-over measurements using a 32 microphone array. It was shown that the outcomes of the simulation and the experiment were very similar. Functional beamforming produces superior acoustic images in terms of both the dynamic range and the resolution for both synthetic and experimental data [6]. In order to use beamforming techniques, measurements must be adequately sampled, which means that the array must have at least twice as many samples as the maximum wavenumber. This is not the case, however, with compressed beamforming, a type of beamforming based on compressive sensing that has gained popularity in recent years due to its capacity to reconstruct sparse signals from a small number of measurements using convex optimisation techniques [11]. Compressive sensing was developed in the signal processing and applied mathematics communities, and it has subsequently produced impressive results in acoustics. It has been used, for instance, to solve the acoustic source localisation problem using acoustic imaging [12], reverberant environment, acoustic response reconstruction [13], and direction-of-arrival estimate [14].

Most of the research on sound source localisation has been focused on acoustic beamforming and

applying beamforming techniques to the acoustic pressure signals. This requires that pressure sensor array is directly put in the acoustic medium to measure the sound pressure. However, there are some engineering applications where placing microphone/hydrophone array in the fluid is not possible or in some situations extremely difficult and costly. Therefore, acoustic source localisation through vibration of a structure is of practical interest. Leclere and Picard [15] introduced a methodology to localise acoustic sources from the measurement of airborne induced vibrations of a thin structure. To do this, the force analysis technique (FAT) was coupled with the ABF. The FAT was used to identify the parietal pressure field exciting the thin structure from vibration measurements and traditional ABF was then applied to the identified parietal pressure for the localisation of acoustic sources. The experimental implementation showed that the parietal pressure field was correctly identified and quantified from the vibration measurements. The drawback of this technique is that it requires coupling of two methods (FAT and ABF) with their own limitations. For example, in the FAT method, the derivative of the fourth order of the displacement should be estimated by finite difference of the acceleration measurements which can result in noise amplification. Further, the beamforming was based on the propagation of plane waves which may not be an accurate representation of the waves emitted by the acoustic source.

The concept of vibroacoustic beamforming (VABF) technique was first introduced within a PhD thesis in INSA-Lyon [16, 17] with the focus on the acoustic detection of defects or leaks (water-sodium reaction) inside a steam generator units of a nuclear reactor. They used VABF technique to detect the presence of an acoustic monopole inside an elastic cylindrical shell by measuring the external shell vibrations. A vibroacoustic model of the fluid-loaded shell was first considered for numerical analysis. The beamforming technique was then applied to radial velocities of the shell. Analysis of the results highlighted how the fluid-loaded shell influences the detection. Finally, a test in a water-filled steel pipe was achieved to experimentally validate the presented approach. One difficulty in the monitoring of steam generators for water leaking into sodium is that leak-induced vibrations can be masked by background noise. Therefore, it is important to take into account the background noise in the analysis and improve the signal-to-noise ratio (SNR) using appropriate beamforming algorithm. Kassab et al. [18] examined this with experimental investigations on a mock-up consisting of a cylindrical pipe coupled with a hydraulic circuit by two flanges. Vibration due to the background noise was controlled by changing the flow speed, and a sound emitter was placed in the pipe to replicate the source to be detected. The signals obtained by an array of accelerometers installed on the pipe were then processed

by beamforming. The conventional type of beamforming was studied, as well as an advanced type based on SNR maximisation (MaxSNR method) [19, 20]. It was discovered that traditional beamforming was ineffective at greater flow rates, which was due to the significant coherence of the vibratory signals created by the turbulent flow, which contradicted the standard beamforming assumption. Using the MaxSNR beamforming, on the other hand, considerable beamforming gain was achieved for various source positions.

Although the VABF has been implemented for leak detection in pipes, it has not been used for acoustic source localisation. This work explores the possibility of source localisation by applying a beamforming technique to the vibration signals measured at the surface of a structure in contact with a fluid domain where the sound source is located. Therefore, it eliminates the need of placing the sensor array directly in the fluid. This is an alternative method to the traditional ABF where sound pressure is measured by a microphone array. In this work, performance of the VABF is evaluated both qualitatively and quantitatively by comparing its source map, dynamic range and spatial resolution with those obtained by the ABF at different frequencies. Moreover, in order to have a more realistic numerical analysis, source localisation is conducted in a noisy environment with different levels of SNR to examine the effectiveness of the VABF. Furthermore, different frequency domain beamforming techniques are applied to the measured signals to localise the source. Performance of each beamforming technique is also demonstrated and the key parameters of the system which is influencing the localisation process are discussed.

2. Frequency Domain Acoustic and Vibroacoustic Beamforming Methods

Figure 1 shows a schematic diagram for source localisation using the acoustic and vibroacoustic beamforming methods. In the former, a flush-mounted microphone array is considered which is the standard configuration for the ABF as shown in Figure 1(a). In this case, the beamforming treatments are performed on the pressure signals measured by the microphones. It is assumed that mounting structure is rigid. Even if the mounting structure was not rigid, since in this work the ABF is conducted in air, the interaction between the acoustic medium and the elastic structure would be weak and can be neglected. Therefore, vibrations of mounting structure have a negligible effect on the pressure measured by the microphones. In the VABF, vibration of the structure due to the acoustic source and noise field excitations is measured by an accelerometer array, and a beamforming technique is

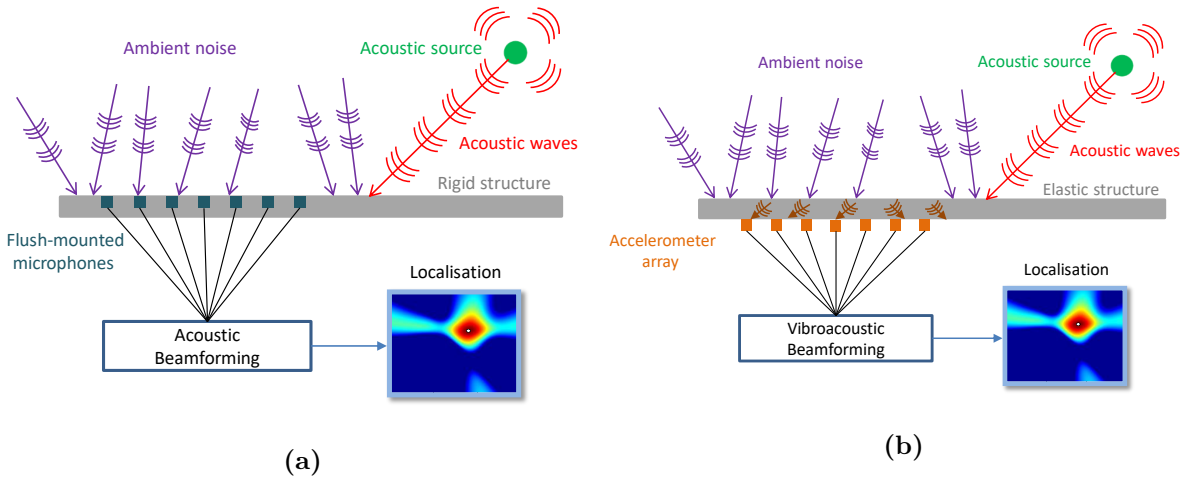

Figure 1: Illustration of an acoustic source localisation in the presence of background noise using (a) a microphone array (acoustic beamforming) and (b) an accelerometer array (vibroacoustic beamforming).

then applied to the vibration data to localise the acoustic source as shown in Figure 1(b). Contrary to the ABF where pressure signals are measured by a microphone array, measured accelerations in the VABF depend on the dynamic behaviour of the mounting structure. In this work, it is assumed that the acoustic source to be localised produces a harmonic deterministic signal whereas the noise is considered to be random and stochastic. Moreover, it should be mentioned that for the purpose of a fair comparison between the ABF and VABF, the number of sensors, their positions and the array pattern are the same in both the ABF and VABF to ensure any differences in the beamforming outputs obtained from these two methods are attributed to their performances and not due to the variation in the system setup and configuration.

In the next sub-section, four widely used beamforming techniques namely conventional, functional, MVDR and MPDR beamformings are herein employed to evaluate the performance of the proposed VABF against the ABF. These techniques can be applied to both the ABF and VABF. For the sake of brevity, they are presented only for the vibroacoustic beamforming in which the array signals correspond to the structural accelerations.

2.1. Beamforming Techniques

2.1.1. Conventional Beamforming

Let us define the CSM of the signals measured by the accelerometers at angular frequency ω by $\mathbf{\Gamma}(\omega)$. For an array of n accelerometers, $\mathbf{\Gamma}$ is an $n \times n$ square matrix where the entry in the i-th row

and the j-th column corresponds to the cross spectrum density (CSD) function of the accelerations between i-th and j-th sensors ($S_{ij}(\omega)$) at frequency ω:

$$\mathbf{\Gamma}(\omega) = [S_{ij}(\omega)], \quad \text{where} \quad i, j = 1, 2..., n, \tag{1}$$

assuming that the signals induced by the acoustic source are independent from those generated by the background noise, matrix $\mathbf{\Gamma}(\omega)$ can be expressed as follows,

$$\mathbf{\Gamma}(\omega) = \mathbf{\Gamma}_{\mathrm{s}}(\omega) + \mathbf{\Gamma}_{\mathrm{n}}(\omega), \tag{2}$$

where $\mathbf{\Gamma}_{\mathrm{s}}(\omega)$ is the CSM of the accelerations only due to the monopole source excitation and $\mathbf{\Gamma}_{\mathrm{n}}(\omega)$ is the CSM of the accelerations produced entirely by the background noise. The spatial filter of beamforming is characterized by so-called weight vector $\mathbf{W}$, which is defined for each focus point u in the detection space. The beamforming output at location u is defined by [19]

$$b_u(\omega) = \mathbf{W}_u^{\dagger}(\omega)\mathbf{\Gamma}(\omega)\mathbf{W}_u(\omega), \tag{3}$$

where the superscript † denotes the Hermitian transpose.

It can be proved that the conventional beamforming output becomes maximum for the actual source location when the weight vector is equal to the well-known steering vector $\mathbf{F}_u$ defined by [17].

$$\mathbf{W}_u(\omega) = \mathbf{F}_u(\omega) = \frac{\mathbf{T}(\omega)}{\|\mathbf{T}(\omega)\|}, \tag{4}$$

where $\| \ \|$ represents the Euclidean norm and $\mathbf{T}(\omega) = [T_{ui}(\omega)]$ is a vector containing the transfer functions for a given focus point u. In other word, the vector component $T_{ui}(\omega)$ is basically the acceleration at the i-th sensor due to the unit source at location u. These transfer functions can be obtained experimentally or by using analytical/numerical models which allow calculating the accelerations of the structure when the system is excited by a monopole source in the acoustic domain. For further details on steering vector selection, see Ref. [21], which studied four distinct steering vector formulations from the literature. None of the formulas were found to give both the correct location and source strength. The various steering vector formulations were demonstrated to be not equally well suited for three-dimensional applications. The steering vector in Eq. (4) is one of two recommended formulations identified in Ref. [21] that allows for accurate source location identification at the cost of a negligible

error in the estimated source strength.

2.1.2. Functional Beamforming

One disadvantage of the CBF is that its source map includes not only the mainlobe (the peak in the source map where the actual source is situated), but also some sidelobes that occur at different locations from the actual source. This is because the computed source distribution is a convolution of the real source distribution and the array's specific response function. Despite the fact that these sidelobes have a lower amplitude than the mainlobe, it is possible that they obscure the source map and make source localisation difficult. The adoption of an improved beamforming algorithm known as functional beamforming is one way to lower the high sidelobe level [10]. In this method, the CSM can be expressed as its eigenvalue decomposition

$$\mathbf{\Gamma}(\omega) = \mathbf{U}\mathbf{\Sigma}\mathbf{U}^{\dagger}, \tag{5}$$

where $\mathbf{U}$ is a unitary matrix whose columns are the eigenvectors of $\mathbf{\Gamma}$, and $\mathbf{\Sigma}$ is a diagonal matrix whose diagonal elements are the eigenvalues of $\mathbf{\Gamma}$. It should be noted that since $\mathbf{\Gamma}$ is a Hermitian matrix, $\mathbf{\Sigma}$ has only real entries. The output of functional beamforming is then given by [22]

$$b_u(\omega) = \left(\mathbf{F}_u^{\dagger}\mathbf{\Gamma}^{\frac{1}{\alpha}}\mathbf{F}_u\right)^{\alpha} = \left(\mathbf{F}_u^{\dagger}\mathbf{U}\mathbf{\Sigma}^{\frac{1}{\alpha}}\mathbf{U}^{\dagger}\mathbf{F}_u\right)^{\alpha}, \tag{6}$$

where parameter α is a real number greater than unity and can be set by the user. When $\alpha = 1$, FBF essentially becomes the CBF as Eqs. (3) and (6) become identical. Using the FBF, sidelobe level or dynamic range μ (typically defined as the difference in dB between the mainlobe and the highest sidelobe) and the array spatial resolution δ (usually defined as the width of the mainlobe 3 dB below its peak) of the source map can be improved for increasing values of α. Common values for α range from 20 to 300. In practice, using well calibrated arrays values of 100 leads to satisfying results [6]. The presence of numerous sidelobes usually becomes a problem, especially at high frequencies. This procedure significantly reduces sidelobes and increases the dynamic range of the results. The computational time required for FBF is almost identical to classical beamforming since the only addition is the effort to perform a spectral decomposition of the CSM.

2.1.3. MVDR Beamforming

MVDR is a typical beamforming algorithm which minimizes the noise in the output power in the desired direction through adjusting a weight factor. The MVDR optimization problem can be expressed as follows

$$\mathbf{W}_u(\omega) = \text{argmin}\left\{\mathbf{W}_u^{\dagger}(\omega)\mathbf{\Gamma}_{\text{n}}(\omega)\mathbf{W}_u(\omega), \quad \text{s.t.} \quad \mathbf{W}_u\mathbf{F}_u = 1\right\}, \tag{7}$$

the solution to this is given by [23]

$$\mathbf{W}_u(\omega) = \frac{\mathbf{\Gamma}_{\text{n}}^{-1}(\omega)\mathbf{F}_u(\omega)}{\mathbf{F}_u^{\dagger}(\omega)\mathbf{\Gamma}_{\text{n}}^{-1}(\omega)\mathbf{F}_u(\omega)}. \tag{8}$$

The MVDR beamformer has higher spatial resolution than a conventional beamformer and its sidelobes are smaller and smoother. However, it requires a matrix inversion every time the noise changes which can be computationally expensive.

2.1.4. MPDR Beamforming

The MVDR beamformer is widely used in applications where it is possible to measure or estimate $\mathbf{\Gamma}_{\text{n}}$. In applications where the signal is always present, the MPDR beamformer is used instead. MPDR is chosen as the optimal solution of

$$\mathbf{W}_u(\omega) = \text{argmin}\left\{\mathbf{W}_u^{\dagger}(\omega)\mathbf{\Gamma}(\omega)\mathbf{W}_u(\omega), \quad \text{s.t.} \quad \mathbf{W}_u\mathbf{F}_u = 1\right\}, \tag{9}$$

this is commonly referred to as Capon's method [24]. Eq. (9) has an analytical solution given by [23]

$$\mathbf{W}_u(\omega) = \frac{\mathbf{\Gamma}^{-1}(\omega)\mathbf{F}_u(\omega)}{\mathbf{F}_u^{\dagger}(\omega)\mathbf{\Gamma}^{-1}(\omega)\mathbf{F}_u(\omega)}. \tag{10}$$

Eq. (9) also differs from Eq. (7) in that the power minimization includes the effect of the desired signal plus noise. The constraint $\mathbf{W}_u\mathbf{F}_u = 1$ in both equations prevents the gain in the direction of the signal from being reduced.

3. Monopole Source Localisation in a Room

In this section, we initially present the configuration of a case study in Section 3.1 which is used to study the localization performance of the VABF against ABF. The vibroacoustic model which is employed to obtain the CSM of the signal and noise as well as the steering vectors is then presented in Section 3.2. A numerical verification based on comparisons with finite element simulations is gathered in Section 3.3. Finally, in Section 3.4, the SNR is formulated in function of the physical characteristics of the case study. This allows us to compare the performance of the VABF with that of the ABF in Section 4 for different values of SNRs (i.e. for different positions of the source).

3.1. Case Study

To demonstrate performance of the vibroacoustic beamforming, let us consider a case study where a monopole source is located in a room. It is assumed all the walls are rigid except a small section of one of the side walls. This small part is chosen to be an elastic rectangular panel with simply supported boundary conditions along all edges which is located in a rigid baffle (the side wall) as shown in Figure 2. A harmonic monopole source pulsating at the angular frequency ω is the source to be localised. The blocked pressure on the plate surface comprises two acoustic fields: the direct acoustic field which is due to the direct sound emitted by the point source, and the reverberant field which is the due to the reflection of the direct sound by the walls. The reverberant field is assumed to be a fully diffuse acoustic field (DAF) which can be modeled analytically.

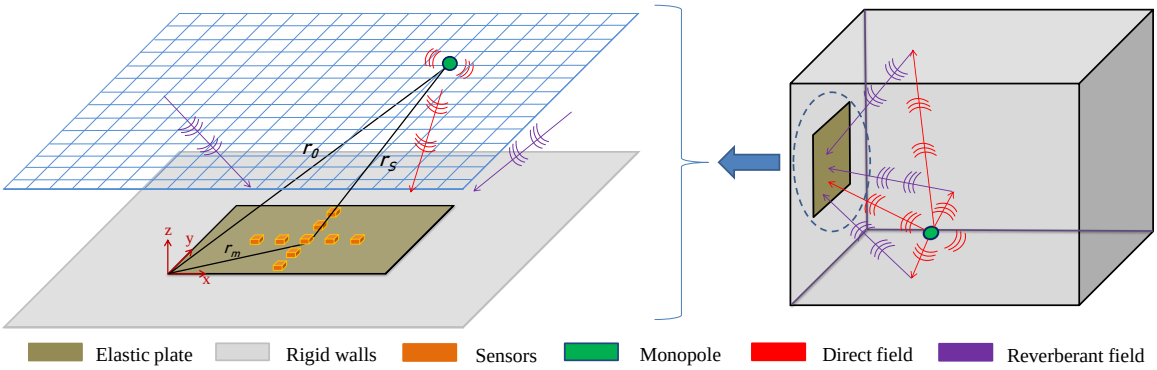

Figure 2: Schematic diagram showing an accelerometer array on a baffled panel under monopole source excitation; beamforming detection space (left), and the baffled panel on the side wall of a rigid room (right).

3.2. Vibroacoustic Beamforming Simulation

The vibroacoustic beamforming outlined in section 2 could be applied to any type of structure. As Eqs. (2) and (3) indicate, the CSD functions of the accelerations between sensors i-th and j-th, S_{ij}, and the transfer functions $T_{ui}(\omega)$ between each sensor and the focus point in the detection space need to be known to calculate the beamforming output. The elements of the CSM can be expressed as the sum of the CSD functions of the accelerations due to the source (S_{ij}^s) and noise (S_{ij}^n) excitations as follows

$$S_{ij}(\omega) = S_{ij}^s(\omega) + S_{ij}^n(\omega), \tag{11}$$

and

$$S_{ij}^s(\omega) = a(\mathbf{x}_i, \mathbf{x}_q, \omega)a^*(\mathbf{x}_j, \mathbf{x}_q, \omega). \tag{12}$$

where $a(\mathbf{x}_i, \mathbf{x}_q, \omega)$ is the acceleration of the structure at i-th sensor due to the monopole source excitation at location q (actual source location). The transfer function is then given by

$$T_{ui}(\omega) = a(\mathbf{x}_i, \mathbf{x}_u, \omega), \tag{13}$$

where $a(\mathbf{x}_i, \mathbf{x}_u, \omega)$ is the acceleration of the structure at i-th sensor due to the monopole source excitation of unit intensity at location u (focus point in the detection space). * indicates complex conjugate. On the other hand, the CSD of the response due to the random noise can be written as [25]

$$S_{ij}^n(\omega) = \frac{1}{4\pi^2}\int_{\infty} H_a^*(\mathbf{x}_i, \mathbf{k}, \omega)\phi_{pp}(\mathbf{k}, \omega)H_a(\mathbf{x}_j, \mathbf{k}, \omega)d\mathbf{k}, \tag{14}$$

where $H_a(\mathbf{x}_i, \mathbf{k}, \omega)$ is the sensitivity function of the structure acceleration excited by a unit wall plane wave. $\phi_{pp}(\mathbf{k}, \omega)$ is the wavenumber-domain CSD of the wall pressure field due to the noise, and $\mathbf{k}$ is the wavevector with components k_x and k_y in the $x-$ and $y-$ directions, respectively.

For the baffled panel with simply supported boundary conditions along its edges, the panel acceleration excited by a monopole source is given by [25]

$$a(\mathbf{x}_i, \mathbf{x}_q, \omega) = -\omega^2 \sum_{m=1}^{M}\sum_{n=1}^{N} \frac{F_{mn}(\mathbf{x}_q)\varphi_{mn}(\mathbf{x}_i)}{\Omega(\omega_{mn}^2 - \omega^2 + \mathrm{j}\eta\omega\omega_{mn})}, \tag{15}$$

where M and N are the cut-off modal orders in the $x-$ and $y-$ directions, respectively. $\mathrm{j} = \sqrt{-1}$

is imaginary unit and $\Omega = \rho_s h L_x L_y/4$ is the modal mass. η is the damping loss factor, ρ_s is panel density, h is panel thickness and L_x, L_y are the panel length and width in the $x-$ and $y-$ directions, respectively. The modal frequencies are given by

$$\omega_{mn} = \sqrt{\frac{D}{\rho_s h}} \left(\left(\frac{m\pi}{L_x} \right)^2 + \left(\frac{n\pi}{L_y} \right)^2 \right), \tag{16}$$

where $D = Eh^3/(12(1-\nu^2))$ is the flexural rigidity, E is the Young's modulus and ν is Poisson's ratio. $\varphi_{mn}(\mathbf{x})$ are the panel mode shapes given by

$$\varphi_{mn}(\mathbf{x}) = \sin\left(\frac{m\pi x}{L_x} \right) \sin\left(\frac{n\pi y}{L_y} \right), \tag{17}$$

and

$$F_{mn}(\mathbf{x}_q) = \int_{\Omega} p(\mathbf{x}_q, \mathbf{x}', \omega) \varphi_{mn}(\mathbf{x}') \mathrm{d}\mathbf{x}', \tag{18}$$

where Ω is the integration domain over the panel surface and $p(\mathbf{x_q}, \mathbf{x}', \omega)$ is the acoustic wall pressure generated by a monopole source given by [26]

$$p(\mathbf{x}_q, \mathbf{x}', \omega) = \frac{\mathrm{j}\rho_0 \omega Q_v}{2\pi r_s} e^{-\mathrm{j}k_0 r_s}, \qquad r_s = |\mathbf{x}_q - \mathbf{x}'|, \tag{19}$$

where Q_v is the source strength, ρ_0 is the fluid density, $k_0 = \omega/c_0$ is the acoustic wavenumber and c_0 is speed of sound in the fluid. Eq. (18) can be numerically computed using rectangular integration method. Once the plate accelerations are computed by Eq. (15), the CSM of signal and transfer functions can be obtained using Eqs. (12) and (13), respectively.

To be able to conduct the beamforming procedure, one also needs to calculate the CSM of noise as expressed by Eq. (14). This requires that the sensitivity function $H_a(\mathbf{x}, \mathbf{k}, \omega)$ and the CSD of noise to be known. The sensitivity function for a simply supported rectangular plate is given by [27]

$$H_a(\mathbf{x}, \mathbf{k}, \omega) = -\omega^2 \sum_{m=1}^{M} \sum_{n=1}^{N} \frac{\psi_{mn}(\mathbf{k}) \varphi_{mn}(\mathbf{x})}{\Omega(\omega_{mn}^2 - \omega^2 + \mathrm{j}\eta\omega\omega_{mn})}, \tag{20}$$

where the modal forces ψ_{mn} are calculated by integration over the panel surface as follows

$$\psi_{mn}(\mathbf{k}) = \int_{\Omega} \varphi_{mn}(\mathbf{x}) e^{-\mathrm{j}(k_x x + k_y y)} \mathrm{d}\mathbf{x} = I_m^x(k_x) I_n^y(k_y), \tag{21}$$

and

$$\{I_s^r(k_r)|(r,s)=(x,m)\vee(y,n)\}=\left\{\begin{array}{ll}\left(\dfrac{s\pi}{L_r}\right)\dfrac{(-1)^s e^{-\mathrm{j}(k_r L_r)}-1}{k_r^2-\left(\dfrac{s\pi}{L_r}\right)^2}, & k_r\neq\dfrac{s\pi}{L_r}\\ \\ \frac{1}{2}\mathrm{j}L_r, & \text{otherwise}\end{array}\right\}. \tag{22}$$

Where $\vee$ is a logical connective which means 'or'. The CSD of the stochastic noise field can be expressed in terms of the auto spectrum density (ASD) function $S_{pp}^{\text{diffuse}}(\omega)$ and the normalized CSD function of the stochastic field $\tilde{\phi}_{pp}(\mathbf{k},\omega)$ as follows [28, 29]

$$\phi_{pp}(\mathbf{k},\omega)=S_{pp}^{\text{diffuse}}(\omega)\tilde{\phi}_{pp}(\mathbf{k},\omega), \tag{23}$$

the normalised CSD function of the DAF in the wavenumber-frequency space is given by [30].

$$\tilde{\phi}_{pp}(k_x,k_y,\omega)=\left\{\begin{array}{ll}\dfrac{2\pi}{k_0\sqrt{k_0^2-k_x^2-k_y^2}}, & k_0^2>k_x^2+k_y^2\\ \\ 0, & k_0^2\leq k_x^2+k_y^2\end{array}\right\}. \tag{24}$$

To compute the CSM of noise, Eq. (14) can now be evaluated numerically using the rectangular integration method. For the DAF excitation, since the normalized CSD function $\tilde{\phi}_{pp}(k_x,k_y,\omega)$ is null for the wavenumbers larger than the acoustic wavenumber, the wavenumber domain of integration in Eq. (14) is basically inside the acoustic circle defined by $\Omega_a=\left\{\mathbf{k}\in\mathbb{R}^2,|\mathbf{k}|<k_0\right\}$. Finally, Eq. (3) can be used to calculate the beamforming output and perform source localisation.

3.3. Model Verification

To verify the mathematical models of the panel under monopole and DAF excitations, the spatial average of the ASD of the panel acceleration under each excitation is analytically computed and is compared with those obtained using the finite element method (FEM) in COMSOL as shown in Figures 3 and 4, respectively. The spatial average of the ASD of the panel acceleration is given by [25]

$$\left\langle a^2\right\rangle=\frac{1}{A_{\mathrm{p}}}\int_{\Omega}S_{aa}(\mathbf{x},\omega)\mathrm{d}\mathbf{x}, \tag{25}$$

where A_p is the surface area of the panel, for the monopole excitation Eq. (25) can be written as follows

$$\left\langle a^2 \right\rangle = \frac{\omega^4}{4} \sum_{m=1}^{M} \sum_{n=1}^{N} \left| \frac{F_{mn}(\mathbf{x}_q)}{\Omega(\omega_{mn}^2 - \omega^2 + \mathrm{j}\eta\omega\omega_{mn})} \right|^2, \tag{26}$$

and for the DAF excitation it can be expressed as [25]

$$\left\langle a^2 \right\rangle = \frac{\omega^4}{16\pi^2} \sum_{i=1}^{N_x} \sum_{j=1}^{N_y} \sum_{m=1}^{M} \sum_{n=1}^{N} \left| \frac{\psi_{mn}(k_x^i, k_y^j)}{\Omega(\omega_{mn}^2 - \omega^2 + \mathrm{j}\eta\omega\omega_{mn})} \right|^2 \phi_{pp}(k_x^i, k_y^j, \omega)\delta k_x \delta k_y, \tag{27}$$

where δk_x and δk_y are the wavenumber resolutions in the k_x and k_y directions, respectively. N_x, N_y are the number of points considered for sampling the wavenumber domain. For numerical analysis, the dimensions and material properties of the panel are listed in Table 1. The fluid density and speed of sound were set to 1.225 kg/m^3 and 343 m/s, respectively. It should be mentioned that the standard

Table 1. Dimensions and material properties of the panel

Parameter	Value
Young's modulus, E (GPa)	70
Poisson's ratio, ν	0.3
Mass density, ρ_s (kg/m^3)	2700
Length, L_x (mm)	480
Width, L_y (mm)	420
Thickness, h_s (mm)	3.2
Damping loss factor, η	0.01

FEM is an element-based method which can be used for analysing a structure under deterministic excitation. It can be directly used for monopole excitation as it is deterministic. However, the DAF excitation is random. Hence, to be able to simulate the plate response under the DAF excitation, the diffuse sound field is defined as a sum of 100 uncorrelated plane waves moving in random directions. The response of the plate to 30 realizations of these deterministic excitation forces are then computed and the final response is obtained by calculating the ensemble average over all the different realizations at each frequency [27, 28]. For this verification, the monopole is located at (x,y,z)=(0.240 m, 0.227 m, 0.017 m) and a unity ASD for the DAF in both models are assumed.

It can be seen from Figures 3 and 4 that analytical results are in excellent agreement with the FEM results particularity in lower frequencies. A small shift in frequency can be observed in the response at higher frequencies between the two predictions. This can be attributed to the fact that the classical plate theory (CPT) is used in the analytical model which ignores transverse shear deformation whereas it was included in the FEM model. It is well known that CPT overestimates the higher natural

frequencies as it is the case for our comparison. However, this is not affecting our numerical analysis for evaluating the beamforming performance in this work. The vertical blue lines in Figures 3 and 4 correspond to the selected frequencies for numerical investigations in the next section, which correspond to one non-resonance frequency (1489 Hz) and three resonance frequencies (1614 Hz, 2425 Hz and 3114 Hz).

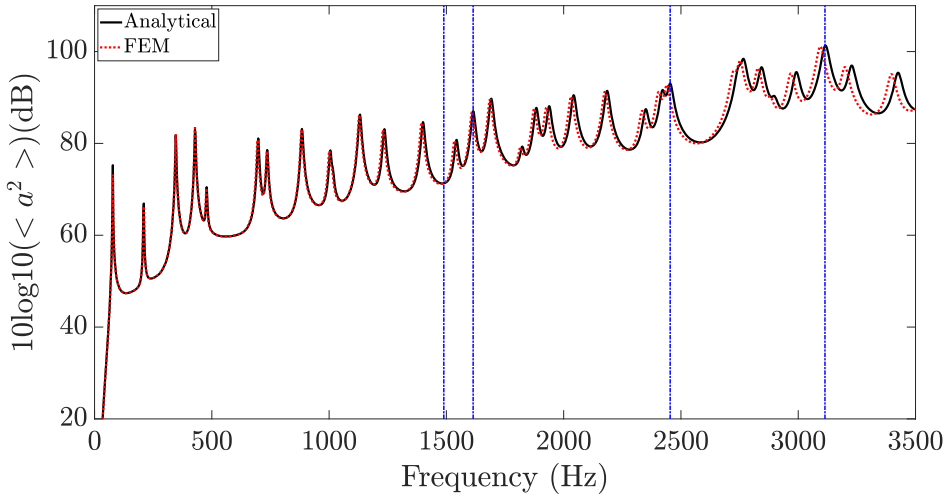

Figure 3: Predicted spatial average of the ASD of the panel acceleration due to monopole excitation (dB ref. 1 $(m/s^2)^2$).

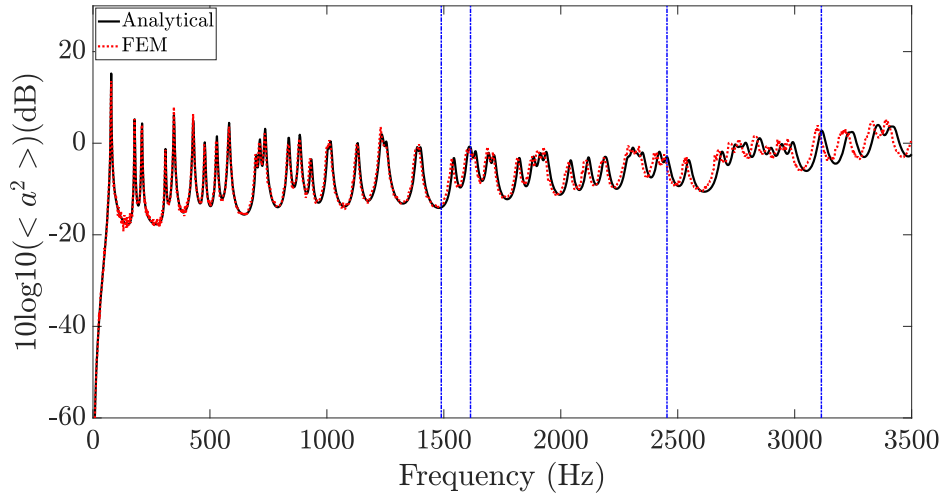

Figure 4: Predicted spatial average of the ASD of the panel acceleration due to DAF excitation (dB ref. 1 $(m/s^2)^2$).

3.4. Signal to Noise Ratio in Function of the Source Distance from the Plate

It is assumed that the sound field in the room is diffuse. One of the properties of this diffuse field is that the sound pressure level is the same for all positions in the room, and there is no preferred sound direction. Although this is roughly fulfilled at frequencies above the Schroeder frequency, we know from experience that as we get close to a source, we can readily hear where the sound comes from and the level increases as we get closer. We are in the immediate field of the source in this situation. Since we have both direct and diffuse fields in a room, the point where both fields have equal strength is the transition between them.

In order to evaluate performance of vibroacoustic beamforming, the numerical results in the next section will be compared against the corresponding results obtained by the acoustic beamforming using a microphone array located on a rigid wall in the room. Therefore, it is appropriate to define the SNR based on the pressure rather than acceleration to be able to achieve such a comparison in the same pressure field condition. Let us define the SNR as the ratio expressed in dB of the ASD of the blocked pressure at the centre of the array due to the direct field induced by the source to be localised, S_{pp}^{direct}, over the ASD of the diffuse field S_{pp}^{diffuse} as follows

$$\text{SNR} = 10\log_{10}\left(\frac{S_{pp}^{\text{direct}}(r_s,\omega)}{S_{pp}^{\text{diffuse}}(\omega)}\right), \tag{28}$$

to express the SNR as a function of the distance between the source and the centre of the array and the room characteristics, one can write S_{pp}^{direct} using Eq. (19) as

$$S_{pp}^{\text{direct}}(r_s,\omega) = p(\mathbf{x}_q,\mathbf{x}',\omega)p^*(\mathbf{x}_q,\mathbf{x}',\omega) = \frac{\rho_0^2\omega^2 Q_v^2}{4\pi^2 r_s^2}, \tag{29}$$

the sound power radiated by a monopole source in an unbounded space is given by [31, 32]

$$W = \frac{Q_v^2\rho_0\omega^2}{8\pi c_0}, \tag{30}$$

Eq. (29) can be then rewritten in terms of sound power as follows

$$S_{pp}^{\text{direct}} = \frac{2\rho_0 c_0 W}{\pi r_s^2}. \tag{31}$$

On the other hand, the ASD of the blocked pressure related to the diffuse field can be expressed as a

function of the sound power and the reverberation time TR_{60} using the Sabine theory [33, 34],

$$S_{pp}^{\mathrm{diffuse}}(\omega) = \frac{50W\rho_0 c_0 \mathrm{TR}_{60}}{V}, \tag{32}$$

where V is the room volume. Using Eqs. (31) and (32), SNR can be finally expressed as

$$\mathrm{SNR} = 10\log_{10}\left(\frac{V}{25\pi r_s^2 \mathrm{TR}_{60}}\right). \tag{33}$$

4. Performance Assessment of the Acoustic Beamforming versus Vibroacoustic Beamforming

To evaluate performance of the proposed VABF for a source localization in a room, its beamforming outputs are compared with those obtained using the ABF. Twenty sensors (microphones/accelerometers) are used in a circular array of radius 95.5 mm which are evenly distanced by 30 mm along the circumference of the circle. To avoid spatial aliasing and adequately sample the vibration data by the sensors for a given wavelength, the distance between the sensors d must satisfy the following criterion:

$$d < \frac{1}{2}\min\left\{\lambda_0, \lambda_f\right\}, \tag{34}$$

where λ_0 and λ_f are the acoustic wavelength and plate flexural wavelength, respectively. Clearly, for the ABF only acoustic wavelength needs to be considered in Eq. (34).

To simulate a realistic condition for SNR calculation, a standard reverberant room with the volume of 147 m^3 and the mean reverberation time of 3.1 s (averaged over the frequency range) are chosen. The SNR in the room is a function of distance between the source and the receiver (centre of the sensor array) as indicated by Eq. (33). It should be noted that to have different SNRs in this work, the source is moved away from the centre of the array in yz-plane along a line which makes 45-degree angle with y/z-axes. Three different scenarios for SNR are herein examined as follows:

- Case 1: SNR=30 dB, which is the case when the source is very close to the receiver (r_s=25 mm). Therefore, the direct field is significantly stronger than reverberant field.

- Case 2: SNR=0 dB, this is the case when the source is at the certain distance from the receiver (r_s=777 mm) such that both fields have the same strength.

- Case 3: SNR=-5 dB, which is the case when the source is further away from the receiver (r_s=1382 mm) and the reverberant field is dominant.

It should be noted that to fully describe the excitation fields for the numerical analysis, first the location of the source (r_s) is determined based on the given SNR using Eq. (33). The ASD of the direct pressure field is then obtained from Eq. (29) for a unit monopole source (i.e. Q_v=1 m^3/s). Finally, the ASD of the DAF pressure is computed from Eqs. (30) and (32), and is applied to both acoustic and vibroacoustic beamformings. It is worth noting that the performance of the beamforming treatments will be independent of the value of the source strength, as the ASD of the direct and diffuse fields are proportional to this value. Hence, only the value of the SNR is important in the numerical investigations.

In what follows, the source maps generated using both the ABF and VABF are presented for three different SNRs as mentioned above. In addition to source maps which are useful for visualization, to quantify the performance of each beamforming technique, spatial resolution (δ) and dynamic range (μ) are computed for each case and are shown above each source map. The dynamic range is herein defined as the difference between the mainlobe and the highest sidelobe in the source map in the detection space, and the array spatial resolution is defined as the width of the mainlobe in the x-direction 3 dB below its peak. The resolution refers to the beamforming technique's capacity to resolve and separate sources that are close together. The dynamic range, also known as sidelobe level, is a measurement of the array's capacity to reject sources coming from directions where the array is not guided. Sidelobes are basically non-focus local maxima that cause misleading peaks and sources in the acoustic map.

4.1. Case 1, SNR=30 dB

Figures 5 and 6 show the source maps of a monopole source for both the ABF and VABF using a circular array obtained by the CBF, FBF, MVDR and MPDR respectively at two distinct frequencies of 1489 Hz and 1614 Hz when SNR=30 dB. The actual source location is shown by a small white cross in the source map. The output of beamforming is normalised so that the mainlobe peak is at 0 dB. According to Figure 5, at the non-resonance frequency of 1489 Hz, dynamic ranges in the VABF is considerably lower than those in the ABF using CBF, FBF, MVDR, and CBF produces the worst sound map with dynamic ranges of 10 dB and 3 dB for the ABF and VABF, respectively. However, we can see that using the MPDR, both the ABF and VABF produce clear sound map with almost the same spatial resolution, and dynamic ranges of 35 dB and 32 dB, respectively.

A similar study is conducted in Figure 6 where a resonance frequency of 1614 Hz is considered. As the two considered frequencies are close to each other, the beamforming outputs obtained using the ABF are very similar as can be seen in Figures 5 and 6. However, unlike the ABF in which a microphone array is used, in the VABF vibration sensors are employed. Therefore, performance of the VABF significantly depends on the dynamic behavior of the structure. It is expected that at resonance frequencies, the VABF performs poorly compared with the ABF due to the strong coherence of the vibratory field, even though the wall pressure field induced by the noise is weakly coherent [19]. This is indeed the case as shown in Figure 7 where the coherence of the vibratory field between all 20 sensors are plotted at 1489 Hz and 1614 Hz. At 1489 Hz, the coherence between any two different accelerometers is low as indicated by blue color, whilst a strong coherence can be observed at 1614 Hz mostly in yellow/orange color spread all over the map. This is why the source localisation is not feasible using the CBF, FBF and it is very difficult via the MVDR due to the low dynamic ranges of 0 dB, 1 dB and 8 dB, respectively. However, the source is easily localised using the VABF via the MPDR technique with a high dynamic range of 28 dB. It is evident from Figures 5 and 6 that if MPDR is used, both the ABF and VABF are able to localise the source with a high dynamic range at both resonance and non-resonance frequencies when the signal (direct acoustic field) is considerably higher than noise (reverberant acoustic field).

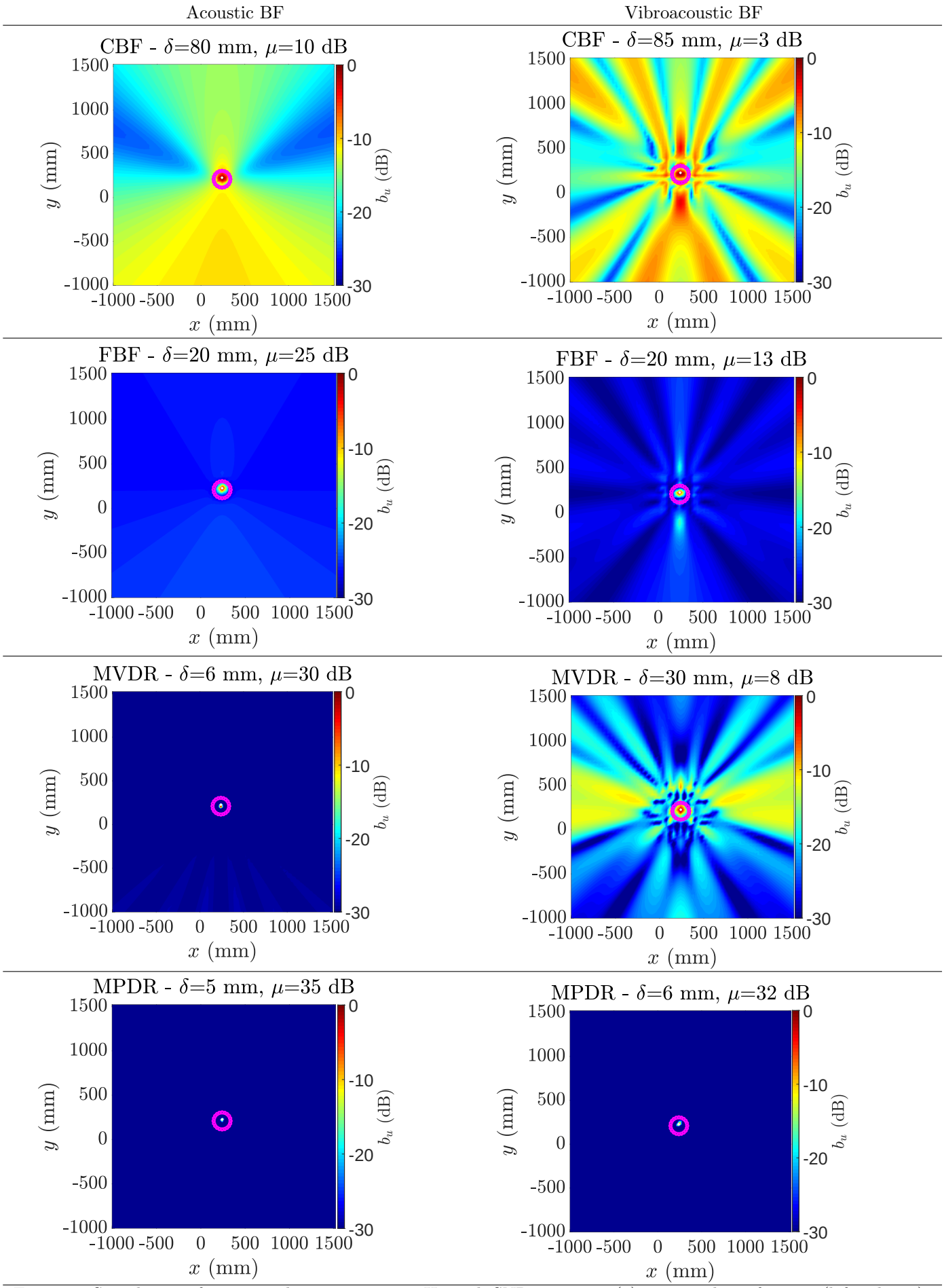

Figure 5. Sound map of a monopole source at 1489 Hz with SNR=30 using (a) acoustic beamforming (left column) and (b) vibroacoustic beamforming (right column) obtained by CBF, FBF, MVDR and MPDR.

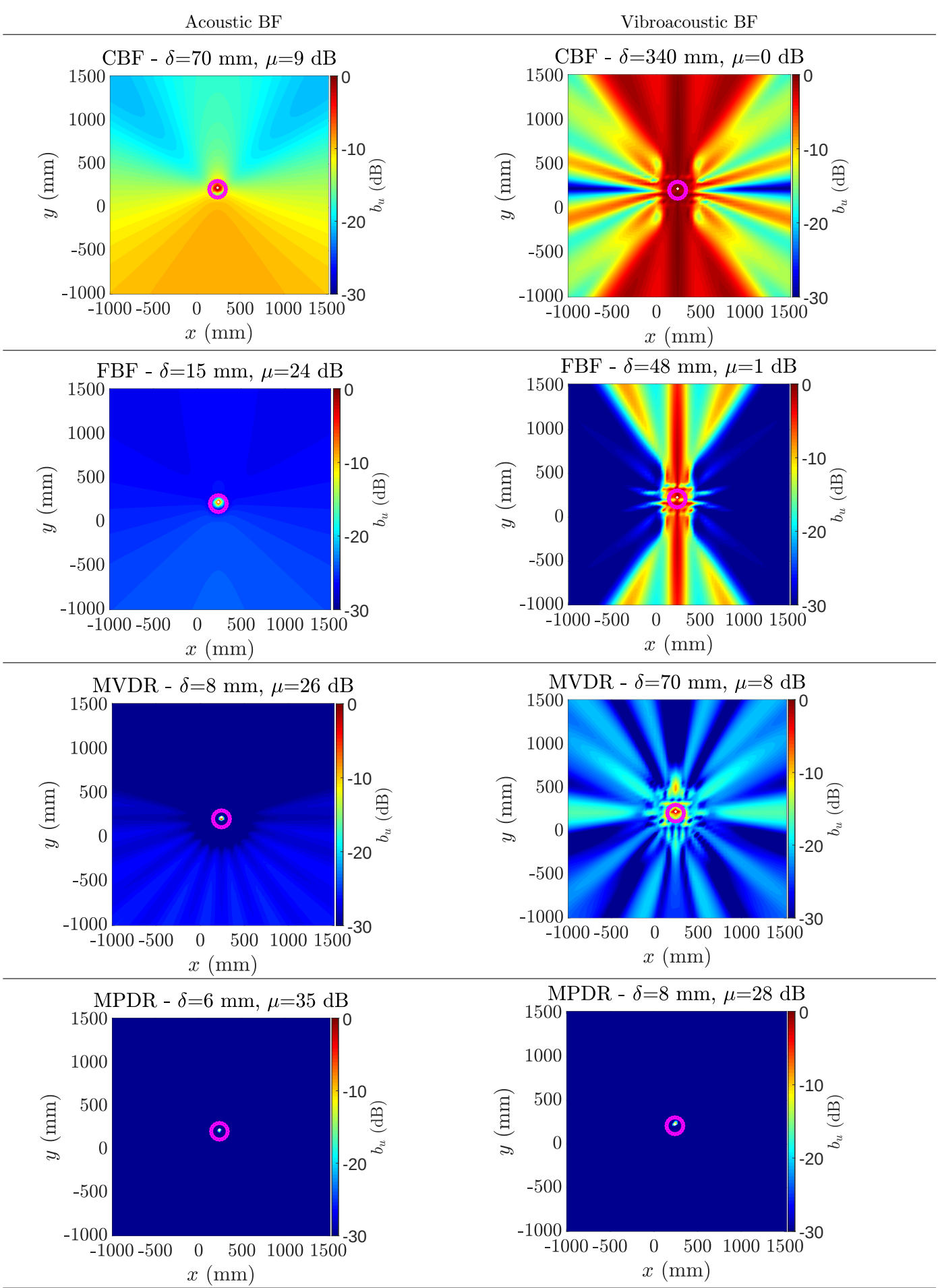

Figure 6. Sound map of a monopole source at 1614 Hz with SNR=30 using (a) acoustic beamforming (left column) and (b) vibroacoustic beamforming (right column) obtained by CBF, FBF, MVDR and MPDR.

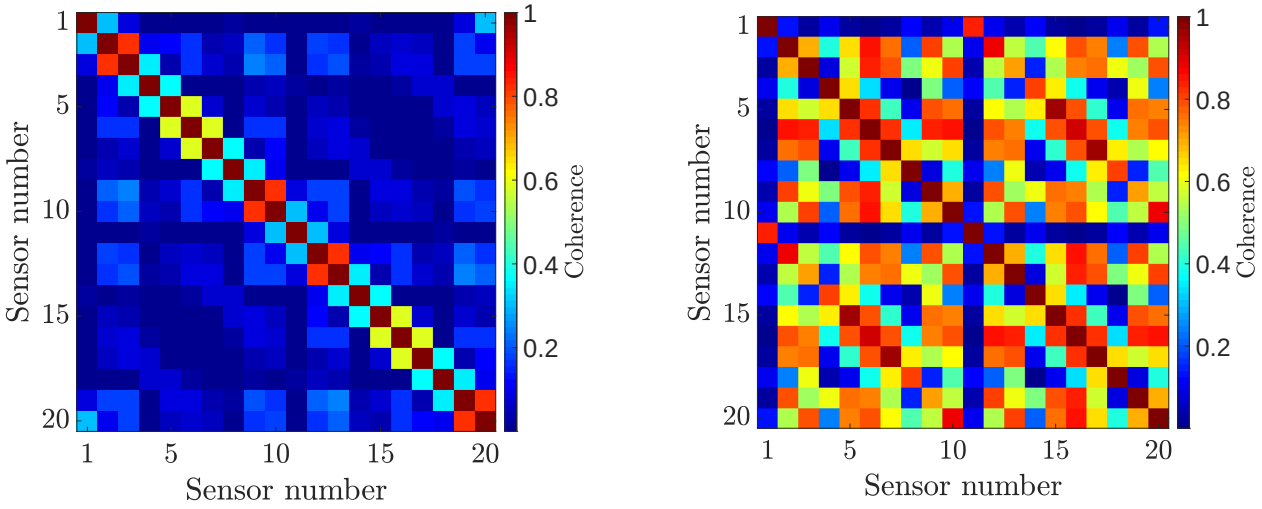

Figure 7. Coherence between 20 accelerometers in the circular array for SNR=30 at frequencies of (a) 1489 Hz and (b) 1614 Hz.

4.2. Case 2 (SNR=0 dB) and Case 3 (SNR=-5 dB)

The studies in Figures 5 and 6 are now repeated for the case when SNR=0 dB as shown in Figures 8 and 9. Figure 8 reveals that at non-resonance frequency of 1489 Hz both the ABF and VABF fail to localise the source when using the CBF or FBF due to very low dynamic range. Although the FBF proved to be able to suppress the sidelobes and improve the sound map quality for SNR=30 dB at 1489 Hz as shown in Figure 5, when the noise level is as high as the signal level, its performance deteriorates. The MPDR continues to provide the most clear sound map in both the ABF and VABF with the dynamic ranges of 8 dB and 7 dB, respectively. As shown in Figure 8, the MPDR in the VABF generates almost the same dynamic range as that in the ABF. However, the spatial resolution achieved by the VABF is nearly half of that obtained in the ABF.

Let us now consider the resonance frequency of 1614 Hz in Figure 9 for SNR=0 dB. It can be observed that at this frequency, both the ABF and VABF perform poorly in particular using the CBF or FBF due to low dynamic range. The dynamic range in the ABF using MVDR is 7 dB which is the same as that in the VABF. It can be seen from both Figures 8 and 9 that for all beamforming techniques except the CBF and FBF, spatial resolutions in the VABF is significantly smaller than those in the ABF when SNR=0 dB. At 1614 Hz, both beamforming methods have the same dynamic range of 7 dB using the MVDR as shown in Figure 8. The dynamic range of the MPDR-based VABF is 3 dB higher than that of the corresponding output in the ABF, and the VABF spatial resolution is less than half of that in the ABF. Hence, localisation is slightly easier using the VABF at this frequency. So far, it has been demonstrated that the MPDR produces the best beamforming output for source localisation. Therefore, we only use this technique for all the subsequent numerical investigations.

Since in the VABF vibration data is collected at the surface of the structure, a question that might arise is that how the structural damping will affect the VABF performance when the excitation frequencies coincide with resonance frequencies of the structure especially at low SNRs. Hence, in the subsequent section the effect of damping on the source localisation is investigated.

4.2.1. Effect of Structural Damping on the Vibroacoustic Beamforming

It is well known that structural damping has a prominent role in the structure response when it is subjected to an excitation at a frequency that is close to a natural frequency. Exactly at resonance, the vibration amplitude becomes substantially large and the vibratory field exhibits strong coherence as demonstrated in Figure 7. The actual amplitude at resonance is controlled solely by the amount of damping. Hence, in this section the effect of damping on the source localisation is investigated. Figure 10 presents the effect of structural damping on the dynamic range and spatial resolution using the MPDR for the circular array at four distinct frequencies of 1489 Hz, 1614 Hz, 2454 Hz and 3114 Hz when SNR=0 dB. The marker symbols correspond to the results for the VABF, while the horizontal lines represents corresponding results for the ABF as they are independent of structural damping.

It is evident from Figure 10(a) that dynamic range in the VABF can be improved by increasing structural damping at all considered frequencies except at 1614 Hz where the dynamic range slightly decreases as structural damping increases. For $\eta \geq 0.1$ the VABF achieves a dynamic range higher than that of the ABF at 1489 Hz, 1614 Hz and 2454 Hz. However, at 3114 Hz, to enhance the VABF dynamic range to the same level as that in the ABF, a damping loss factor of 0.4 is required. It should be noted that the overall dynamic range is low for both methods when SNR=0 dB, for example, by having a loss factor of 0.3, one could achieve a similar dynamic range (1 dB difference) for both methods at 3114 Hz. Moreover, by further increasing the loss factor, the dynamic range converges to a certain value for higher loss factors at all frequencies. It is also observed that the effect of damping loss factor on the dynamic range is greater at higher resonance frequencies. For example, increasing damping loss factor from 0.02 to 0.14 has almost doubled the dynamic range at frequency of 2454 Hz as shown in Figure 10(a). This behavior is attributed to the coherence reduction of the vibratory field due to the high damping loss factor. Figure 11 presents the coherence between different accelerometers for two different loss factors of 0.01 and 0.3 at 2454 Hz. It can be seen that the coherence is considerably reduced by increasing the loss factor from 0.01 to 0.3.

Figure 10(b) shows the spatial resolution as a function of damping loss factor. This figure indicates that the spatial resolution obtained from the VABF is considerably smaller than that in the ABF.

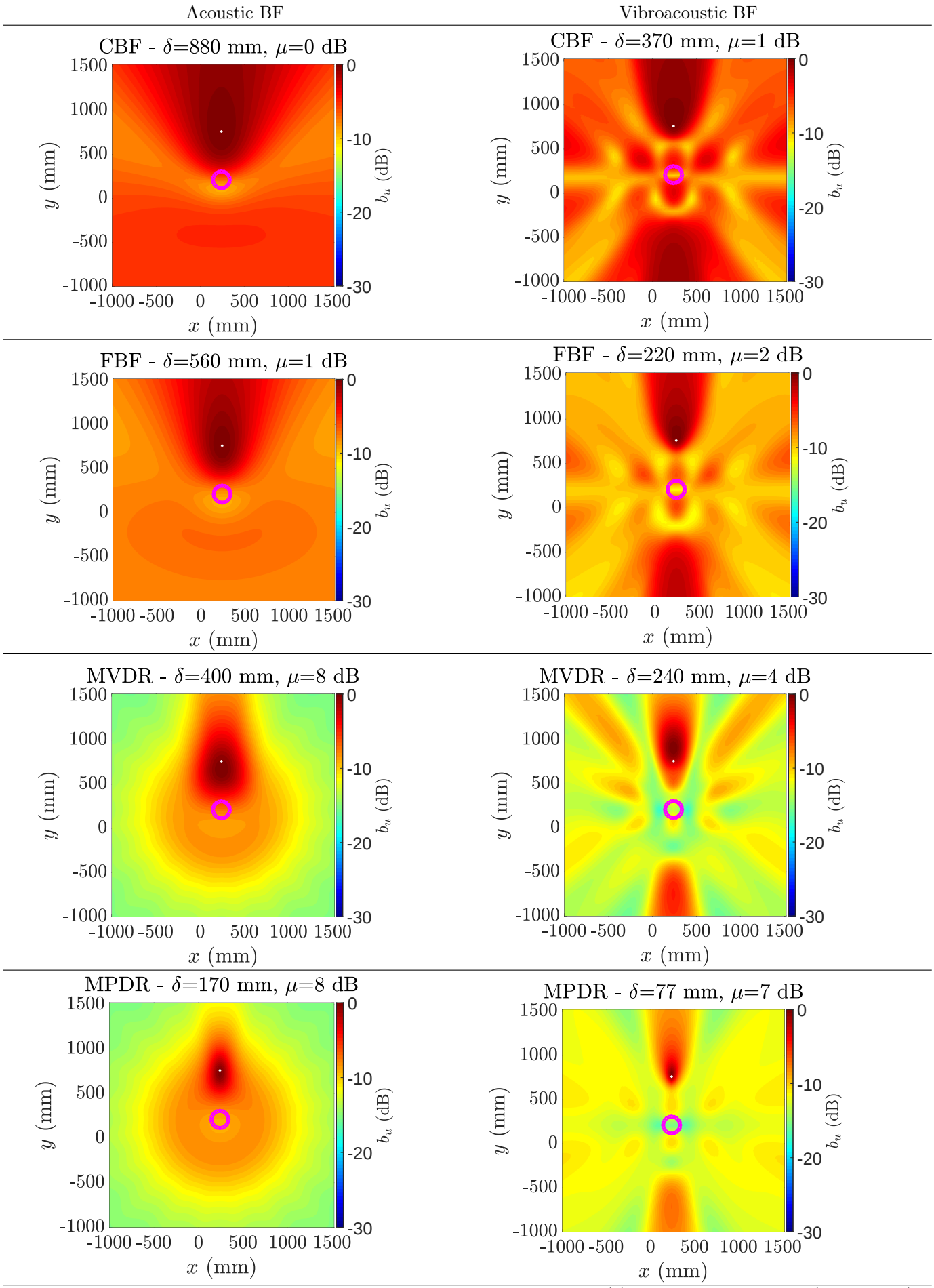

Figure 8. Sound map of a monopole source at 1489 Hz with SNR=0 using (a) acoustic beamforming (left column) and (b) vibroacoustic beamforming (right column) obtained by CBF, FBF, MVDR and MPDR.

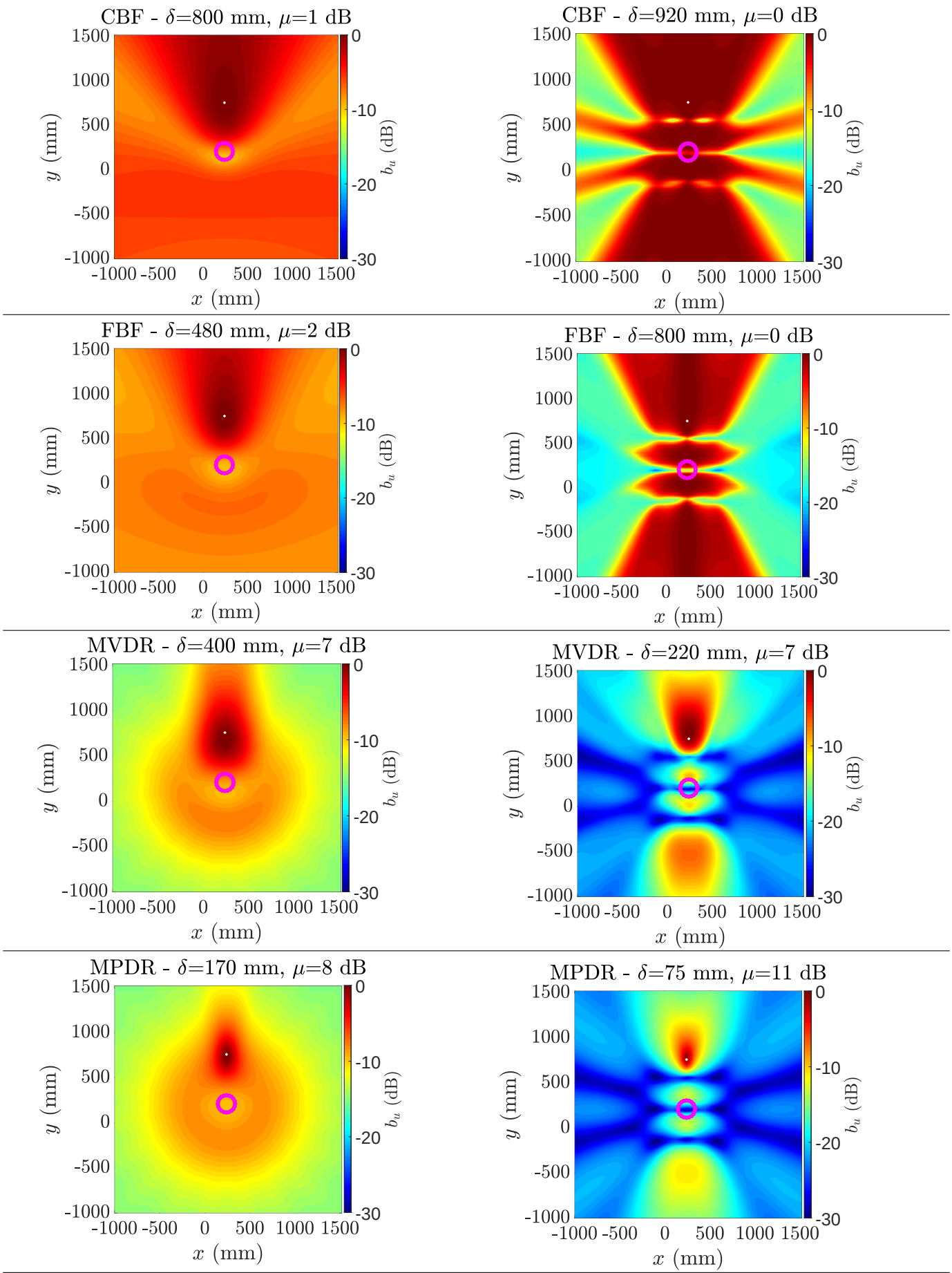

Figure 9. Sound map of a monopole source at 1614 Hz with SNR=0 using (a) acoustic beamforming (left column) and (b) vibroacoustic beamforming (right column) obtained by CBF, FBF, MVDR and MPDR.

This was also demonstrated in Figures 8 and 9. Moreover, increasing structural damping adversely affect the spatial resolution. However, regardless of the damping value, the VABF spatial resolution is always smaller than that in the ABF. The spatial resolution is also converging to a certain value as damping increases.

To further examine the performance of the VABF for low SNRs and to visualize the source map of the VABF for higher structural damping, the VABF outputs at frequencies of 1489 Hz, 1614 Hz, 2454 Hz and 3114 Hz with $\eta = 0.3$ and SNR=0 dB or -5 dB are compared with corresponding outputs using the ABF in Figures 12 and 13, respectively. Generally, a more clear sound map can be generated using the VABF compared with the map obtained using the ABF for both SNRs at most considered frequencies. When SNR=0 dB, the dynamic ranges and spatial resolutions of the ABF are respectively 7-10 dB and 125-170 mm, whilst using the VABF corresponding values are 9-10 dB and 80-96 mm. This behavior holds true for SNR=-5 dB where the dynamic ranges of the VABF are very similar to those of the ABF with significantly smaller spatial resolutions. For SNR=-5 dB that noise level is higher than the direct acoustic field, both beamforming methods fail to localise the source due to the low dynamic range and the presence of pronounced sidelobe contamination in the sound map at all considered frequencies. According to Figures 12 and 13, by choosing an appropriate damping loss factor, one can acquire a similar performance in source localisation using the VABF compared with that of the ABF at low SNRs.

4.3. Effect of Array Pattern on the Vibroacoustic Beamforming

Figure 14 presents the source map of a monopole source using three different array patterns namely circular, cross and random patterns at frequency of 3114 Hz using the ABF and VABF for SNR=-5 dB. The damping loss factor is set to $\eta = 0.3$. In all three cases, 20 sensors are employed and the criterion in Eq. (34) is respected. The size of the array is kept almost the same for different patterns. It is apparent from this figure that the circular and random arrays provide the same dynamic range for the VABF but the cross array has slightly lower dynamic range. The best beamforming output for the ABF is generated using the random array. Although using different array pattern slightly changes the beamforming performance at different frequencies, based on the data in Figure 14 both beamforming methods exhibit roughly similar performance using different array pattern. It should be noted that although a circular array was used for numerical analysis and evaluation of the VABF performance in the previous sections, the same conclusions can be drawn using other array patterns.

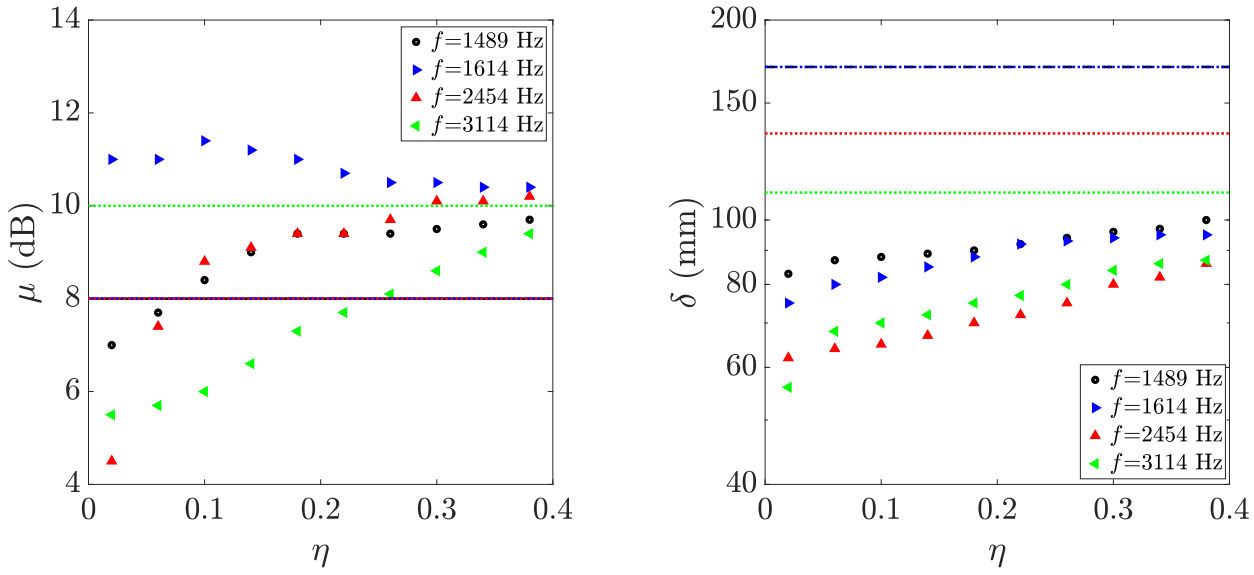

(a) **(b)**

Figure 10. Effect of structural damping on (a) dynamic range and (b) spatial resolution of the vibroacoustic beamforming for a circular array using MPDR at four distinct frequencies of 1489 Hz, 1614 Hz, 2454 Hz and 3114 Hz; the horizontal lines represent the corresponding dynamic range and spatial resolution using the acoustic beamforming.

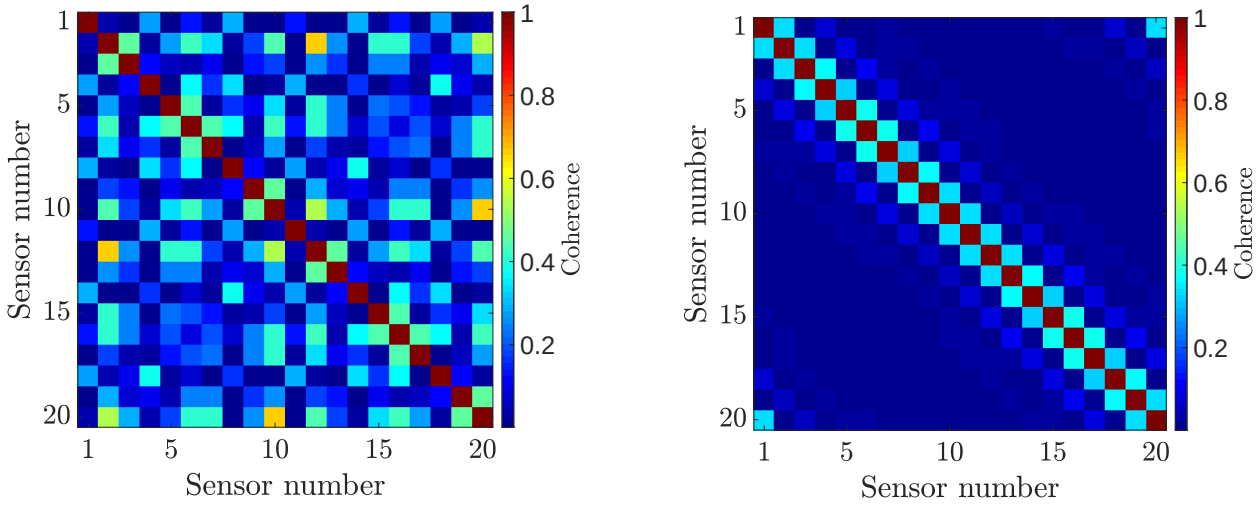

(a) **(b)**

Figure 11. Coherence between 20 accelerometers in the circular array for SNR=0 at frequency of 2454 Hz (a) η=0.01 and (b) η=0.3.

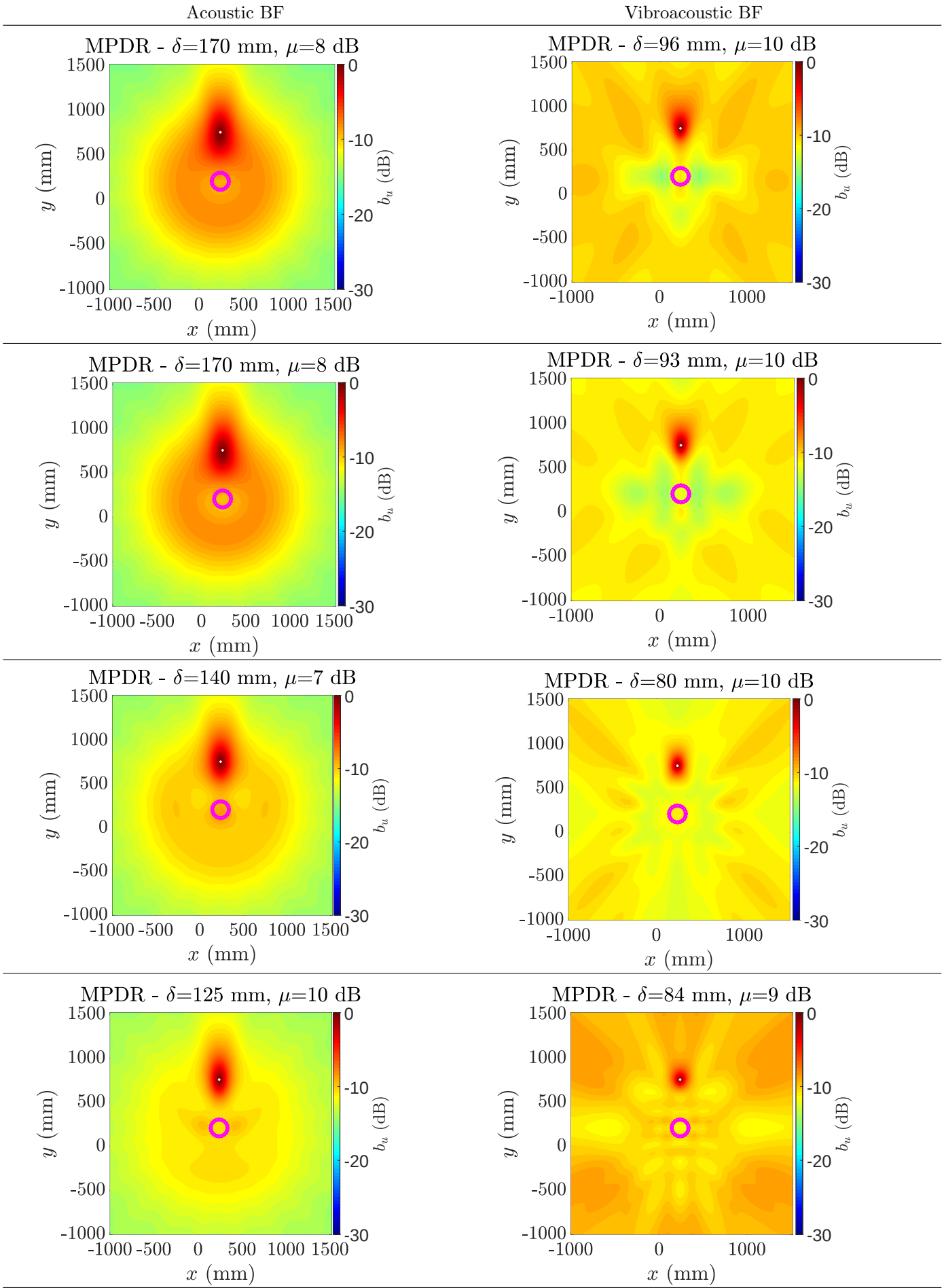

Figure 12. Sound map of a monopole source at 1489 Hz, 1614 Hz, 2454 Hz and 3114 Hz (1st-4th rows, respectively) with SNR=0 using (a) acoustic beamforming (left column) and (b) vibroacoustic beamforming (right column) with a loss factor of 0.3 obtained by MPDR.

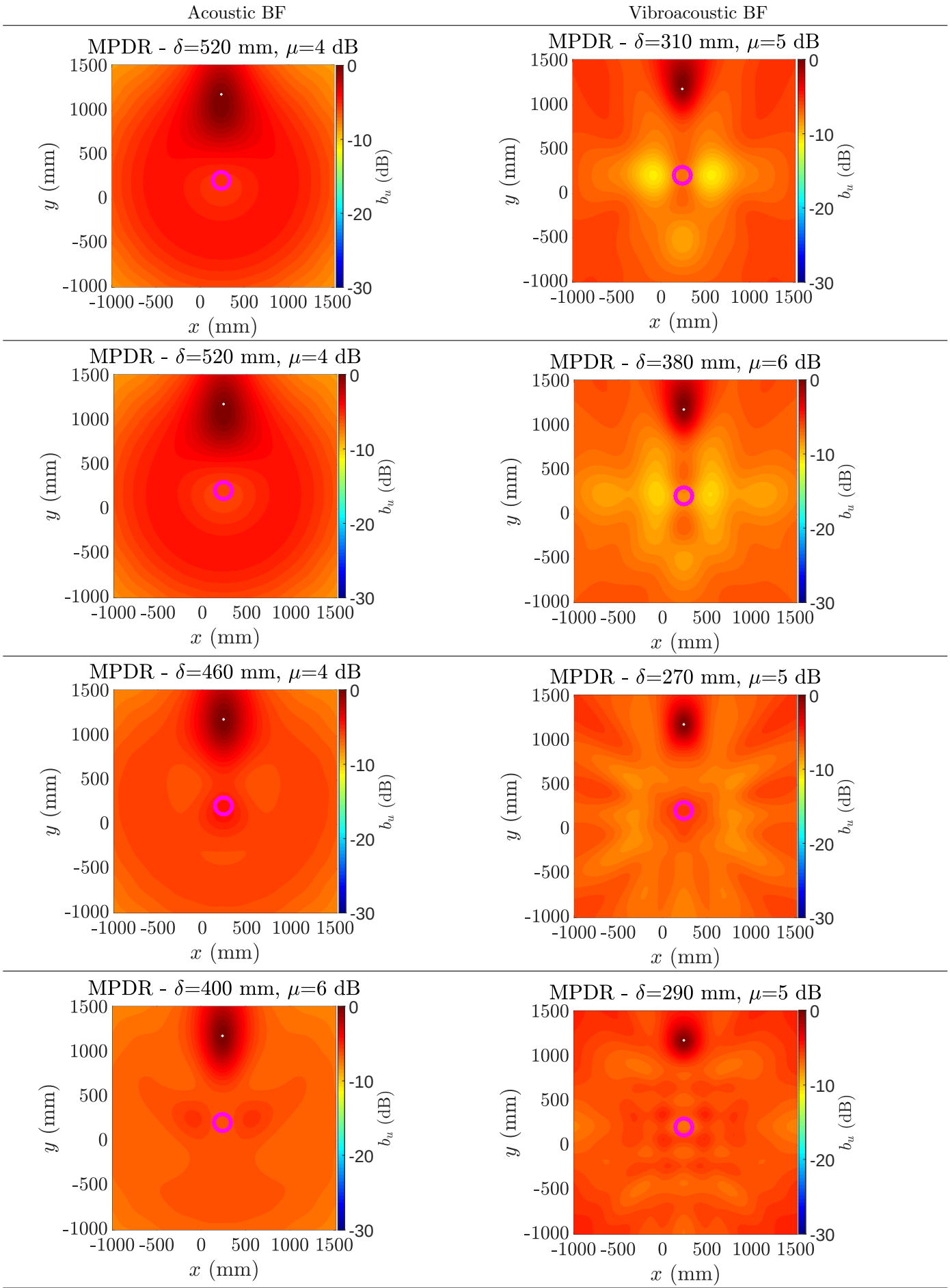

Figure 13. Sound map of a monopole source at 1489 Hz, 1614 Hz, 2454 Hz and 3114 Hz (1st-4th rows, respectively) with SNR=-5 using (a) acoustic beamforming (left column) and (b) vibroacoustic beamforming (right column) with a loss factor of 0.3 obtained by MPDR.

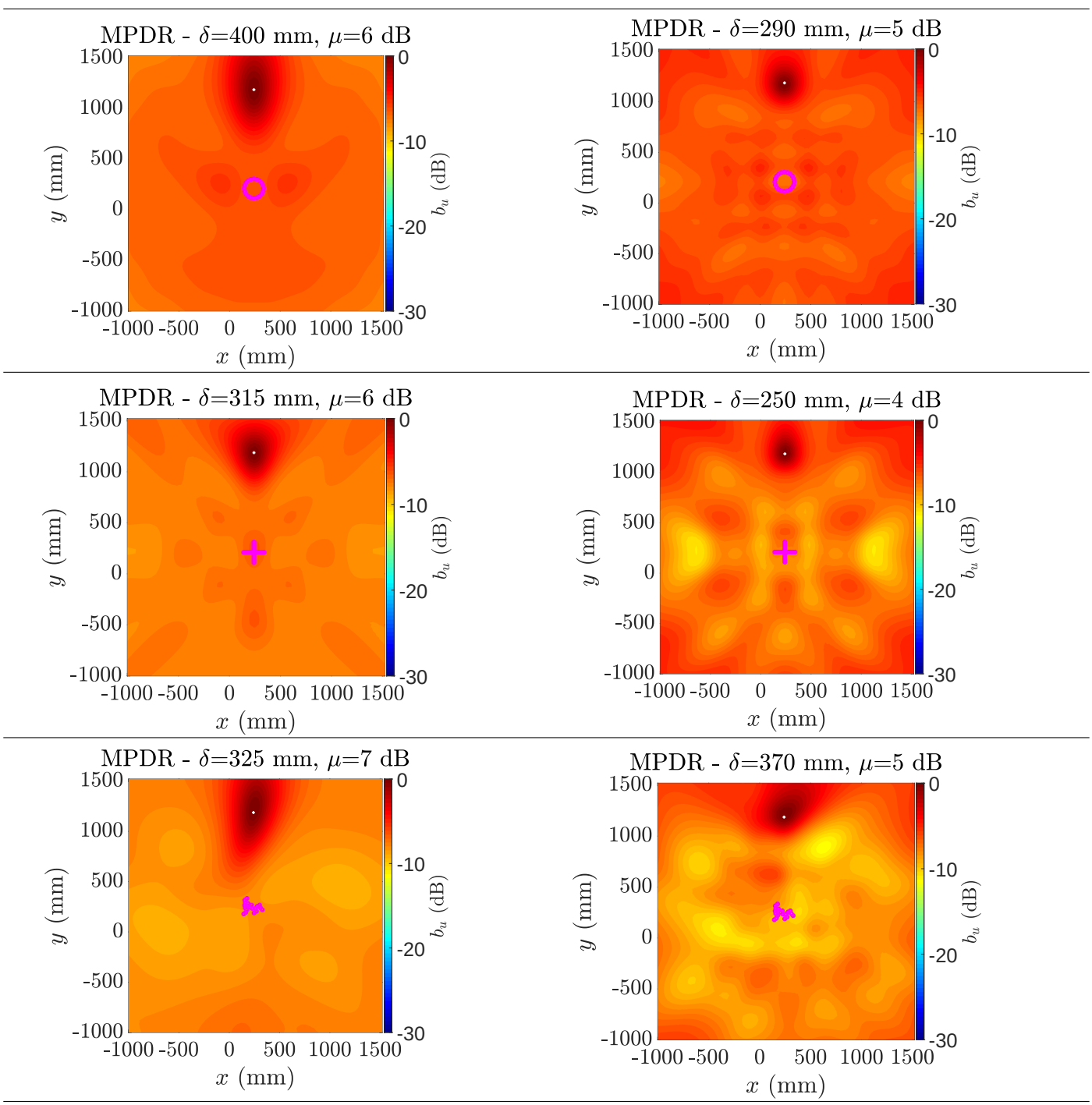

Figure 14. Sound map of a monopole source at 3114 Hz with SNR=-5 obtained by circular, cross and random arrays using (a) acoustic beamforming (left column) (b) vibroacoustic beamforming (right column) with a loss factor of 0.3 obtained by MPDR.

434

5. Conclusions

A vibroacoustic beamforming was proposed for localising an acoustic source using vibration data. This approach is an alternative to the traditional acoustic beamforming where a microphone/hydrophone array has to be placed in the acoustic medium and beamforming algorithm is then applied to measured pressure signal. VABF can be useful when it is not feasible to put the sensor array in the fluid. As the beamforming techniques are applied to the vibration data, the sensor array could be outside the targeted acoustic medium and can be mounted on the structure that is in contact with the fluid in which a source needs to be localised. The proposed method was applied to source localisation in a room. Performance of the VABF was examined by employing CBF, FBF, MVDR and MPDR and comparing the predicted results with corresponding data obtained from the ABF prediction. It was demonstrated that the MPDR produces the highest dynamic range and the clearest source map in both the ABF and VABF at all considered frequencies.

It was also shown that when SNR is high, the MPDR-based VABF can be applied to the vibration response from a structure with a small damping to achieve similar beamforming output for source localisation to that of the MPDR-based ABF. This does not hold true for source localisation when SNR is zero or negative as the source map becomes contaminated with sidelobes and the VABF underperforms. However, it was confirmed that this underperformance can be compensated by increasing the structural damping, which results in reducing the coherence of the vibratory field and consequently enhances the dynamic range in the VABF to the same level or even higher than that in the ABF. Moreover, whilst increasing the damping loss factor also widens the spatial resolution in the VABF, it always remains below the corresponding value in the ABF. Hence, it can be concluded that by applying the VABF to the vibration data from a structure with moderate damping, a similar performance in source localisation to that in the ABF can be accomplished at any SNR. It is worth noting that in order to optimise the performance of the VABF for low SNRs in the frequency range of interest, the proposed numerical study can be employed at the design stage of the mounting structure (plate) to estimate the minimum value of the damping loss factor (eventually in function of the frequency) which is needed to obtain the targeted performance. Accordingly, viscoelastic layers can then be produced and glued on the surface of the structure to reach the required damping.

References

[1] P. Chiariotti, M. Martarelli, P. Castellini, Acoustic beamforming for noise source localization–reviews, methodology and applications, Mechanical Systems and Signal Processing 120 (2019) 422–448.

[2] T. Padois, O. Doutres, F. Sgard, A. Berry, Time domain localization technique with sparsity constraint for imaging acoustic sources, Mechanical Systems and Signal Processing 94 (2017) 85–93.

[3] C. Noël, V. Planeau, D. Habault, A new temporal method for the identification of source directions in a reverberant hall, Journal of sound and vibration 296 (3) (2006) 518–538.

[4] T. F. Brooks, W. M. Humphreys, A deconvolution approach for the mapping of acoustic sources (damas) determined from phased microphone arrays, Journal of sound and vibration 294 (4-5) (2006) 856–879.

[5] H. L. Van Trees, Optimum array processing: Part IV of detection, estimation, and modulation theory, John Wiley & Sons, 2004.

[6] R. Merino-Martínez, M. Snellen, D. G. Simons, Functional beamforming applied to imaging of flyover noise on landing aircraft, Journal of Aircraft 53 (6) (2016) 1830–1843.

[7] L. Ehrenberg, S. Gannot, A. Leshem, E. Zehavi, Sensitivity analysis of mvdr and mpdr beamformers, in: 2010 IEEE 26-th Convention of Electrical and Electronics Engineers in Israel, IEEE, 2010, pp. 000416–000420.

[8] Y. Xiao, J. Yin, H. Qi, H. Yin, G. Hua, Mvdr algorithm based on estimated diagonal loading for beamforming, Mathematical Problems in Engineering 2017.

[9] B. D. Carlson, Covariance matrix estimation errors and diagonal loading in adaptive arrays, IEEE Transactions on Aerospace and Electronic systems 24 (4) (1988) 397–401.

[10] R. P. Dougherty, Functional beamforming for aeroacoustic source distributions, in: 20th AIAA/CEAS aeroacoustics conference, 2014, p. 3066.

[11] P. Gerstoft, C. F. Mecklenbräuker, W. Seong, M. Bianco, Introduction to compressive sensing in acoustics, The Journal of the Acoustical Society of America 143 (6) (2018) 3731–3736.

[12] P. Simard, J. Antoni, Acoustic source identification: Experimenting the l1 minimization approach, Applied Acoustics 74 (7) (2013) 974–986.

[13] J. Le Roux, P. T. Boufounos, K. Kang, J. R. Hershey, Source localization in reverberant environments using sparse optimization, in: 2013 IEEE International Conference on Acoustics, Speech and Signal Processing, IEEE, 2013, pp. 4310–4314.

[14] G. F. Edelmann, C. F. Gaumond, Beamforming using compressive sensing, The Journal of the Acoustical Society of America 130 (4) (2011) EL232–EL237.

[15] Q. Leclère, C. Picard, Acoustic beamforming through a thin plate using vibration measurements, The Journal of the Acoustical Society of America 137 (6) (2015) 3385–3392.

[16] J. Moriot, Passive vibro-acoustic detection of a sodium-water reaction in a steam generator of a sodium-cooled fast neutrons nuclear reactor by beam forming, Tech. rep., Institut National des Sciences Appliquees de Lyon (2013).

[17] J. Moriot, L. Maxit, J.-L. Guyader, O. Gastaldi, J. Périsse, Use of beamforming for detecting an acoustic source inside a cylindrical shell filled with a heavy fluid, Mechanical Systems and Signal Processing 52 (2015) 645–662.

[18] S. Kassab, F. Michel, L. Maxit, Water experiment for assessing vibroacoustic beamforming gain for acoustic leak detection in a sodium-heated steam generator, Mechanical Systems and Signal Processing 134 (2019) 106332.

[19] L. Maxit, M. Karimi, O. Guasch, Spatial coherence of pipe vibrations induced by an internal turbulent flow, Journal of Sound and Vibration 493 (2021) 115841.

[20] L. Maxit, M. Karimi, O. Guasch, F. Michel, Numerical analysis of vibroacoustic beamforming gains for acoustic source detection inside a pipe conveying turbulent flow, Mechanical Systems and Signal Processing 171 (2022) 108888.

[21] E. Sarradj, Three-dimensional acoustic source mapping with different beamforming steering vector formulations, Advances in Acoustics and Vibration 2012.

[22] S. Gombots, J. Nowak, M. Kaltenbacher, Sound source localization–state of the art and new inverse scheme, e & i Elektrotechnik und Informationstechnik (2021) 1–15.

[23] R. G. Lorenz, S. P. Boyd, Robust minimum variance beamforming, IEEE transactions on signal processing 53 (5) (2005) 1684–1696.

[24] J. Capon, High-resolution frequency-wavenumber spectrum analysis, Proceedings of the IEEE 57 (8) (1969) 1408–1418.

[25] M. Karimi, P. Croaker, L. Maxit, O. Robin, A. Skvortsov, S. Marburg, N. Kessissoglou, A hybrid numerical approach to predict the vibrational responses of panels excited by a turbulent boundary layer, J Fluid Struct 92 (2020) 102814.

[26] M. Karimi, L. Maxit, V. Meyer, S. Marburg, R. Kirby, Non-negative intensity for planar structures under stochastic excitation, Journal of Sound and Vibration 488 (2020) 115652.

[27] M. Karimi, L. Maxit, P. Croaker, O. Robin, A. Skvortsov, S. Marburg, N. Atalla, N. Kessissoglou, Analytical and numerical prediction of acoustic radiation from a panel under turbulent boundary layer excitation, Journal of Sound and Vibration (2020) 115372.

[28] L. Maxit, Simulation of the pressure field beneath a turbulent boundary layer using realizations of uncorrelated wall plane waves, J Acoust Soc Am 140 (2) (2016) 1268–1285.

[29] W. Graham, A comparison of models for the wavenumber–frequency spectrum of turbulent boundary layer pressures, J Sound Vib 206 (4) (1997) 541–565.

[30] C. Marchetto, L. Maxit, O. Robin, A. Berry, Vibroacoustic response of panels under diffuse acoustic field excitation from sensitivity functions and reciprocity principles, J Acoust Soc Am 141 (6) (2017) 4508–4521.

[31] D. A. Russell, J. P. Titlow, Y.-J. Bemmen, Acoustic monopoles, dipoles, and quadrupoles: An experiment revisited, American Journal of Physics 67 (8) (1999) 660–664.

[32] M. Karimi, R. Kinns, N. Kessissoglou, Radiated sound power from near-surface acoustic sources, Journal of Ship Research 66 (02) (2022) 151–158.

[33] M. Long, Architectural acoustics, Elsevier, 2005.

[34] J.-D. Chazot, O. Robin, J.-L. Guyader, N. Atalla, Diffuse acoustic field produced in reverberant rooms: A boundary diffuse field index, Acta Acustica united with Acustica 102 (3) (2016) 503–516.